Journal of *Marine Science and Engineering*

MDPI

Article

Local Marine Geomagnetic Anomaly Model Reconstruction via Multi-Source Data Fusion Based on Fully Connected Neural Network

Mengya Wang [1,2], Lin Wu [1,2,*], Zhikuan Pan [1,2], Shi Liu [1,2], Qianqian Li [3], Lifeng Bao [1,2] and Yong Wang [1,2]

[1] State Key Laboratory of Precision Geodesy, Innovation Academy for Precision Measurement Science and Technology, Chinese Academy of Sciences, Wuhan 430077, China; wangmengya@apm.ac.cn (M.W.); panzhikuan@apm.ac.cn (Z.P.); liushi@apm.ac.cn (S.L.); baolifeng@apm.ac.cn (L.B.); ywang@apm.ac.cn (Y.W.)
[2] University of the Chinese Academy of Sciences, Beijing 100049, China
[3] School of Computer and Artificial Intelligence, Hubei University of Education, Wuhan 430205, China; 15072418205@whigg.ac.cn
* Correspondence: linwu@apm.ac.cn

Abstract

The geomagnetic reference map is an important component of underwater geomagnetic matching navigation, and it directly affects navigation and positioning accuracy. However, representative global geomagnetic models still cannot fully meet the requirements of high-precision matching navigation. To address this, this study proposes a local marine geomagnetic anomaly model reconstruction method via multi-source data fusion based on a fully connected neural network. The proposed MAG-DFN method uses the EMAG2 model as the background field and learns model residuals from shipborne measurements to reconstruct the geomagnetic model. Two sub-areas in the South China Sea and the western Pacific were selected for this experiment, each containing two withheld 1° × 1° validation blocks, and four baseline methods were introduced for comparison. The results show that MAG-DFN reduces MAE by 14.71%, 23.35%, 22.09%, and 8.96%, and RMSE by 12.41%, 18.87%, 16.73%, and 6.65%, in the four validation blocks, respectively. In addition, MAG-DFN outperforms all baseline methods. These results indicate that the MAG-DFN method, by integrating high-precision shipborne data, can effectively reduce the local deviations of the EMAG2 and better support matching navigation.

Keywords: underwater geomagnetic matching navigation; multi-source data fusion; fully connected neural network; local marine geomagnetic anomaly model reconstruction

Check for updates

Academic Editor: Gianluca Quarta

Received: 10 September 2026
Revised: 25 October 2026
Accepted: 28 October 2026
Published: 29 October 2026

Copyright: © 2026 by the authors. Licensee MDPI, Basel, Switzerland. This article is an open access article distributed under the terms and conditions of the Creative Commons Attribution (CC BY) license.

1. Introduction

The geomagnetic field is a fundamental physical field of the Earth, and the marine geomagnetic field constitutes an important component of the marine environment. Geomagnetic information is characterised by passivity, non-radiation, and strong resistance to interference, providing robustness against external disturbances and excellent concealment. In recent years, marine geomagnetic information has been incorporated into underwater passive navigation systems to assist inertial navigation systems, aiming to improve the reliability and accuracy of underwater navigation systems. Underwater geomagnetic matching navigation is one of the key technologies in the field of long-endurance underwater passive navigation [1,2]. The geomagnetic reference map is a critical component of the geomagnetic matching navigation system, directly influencing the accuracy of navigation.

The construction of a high-precision geomagnetic reference map determines the baseline accuracy of navigation and positioning [3,4].

Currently, widely used global main geomagnetic field models, such as the IGRF and WMM, have been expanded to spherical harmonic degrees and orders of several tens. However, these models primarily represent the main geomagnetic field with spatial resolutions on the order of thousands of kilometres. Consequently, their accuracy in characterising regional geomagnetic fields is relatively low, making them inadequate for high-precision navigation and positioning requirements [5–7]. In contrast, the magnetic anomaly field is considered to be more suitable for navigation. The global magnetic anomaly model EMAG2 is one of the most accurate geomagnetic anomaly models currently available. It is a gridded dataset of total magnetic intensity anomalies, compiled from satellite, ship, and airborne magnetic measurements provided by research institutions worldwide, with the WGS84 reference ellipsoid and a spatial resolution of 2′ × 2′ [8]. This model has been widely used in studies such as deep geological structure inversion, mineral resource exploration, and geomagnetic matching navigation. However, although the EMAG2 model has incorporated a substantial volume of new marine and airborne geomagnetic data, it has primarily reduced data gaps in certain regions of earlier geomagnetic anomaly models. Its spatial resolution remains at 2′, which limits its ability to represent local geomagnetic anomalies in marine areas, resulting in relatively large errors in some regions [9,10]. Geomagnetic navigation and positioning require high-precision, high-resolution geomagnetic field models. However, current global geomagnetic anomaly models still fall short of meeting these requirements and are insufficient for underwater geomagnetic-aided matching navigation.

Traditional interpolation methods, such as the classical Kriging algorithm and its variants [11,12], and radial basis function methods [13], have been well established in geomagnetic data interpolation and reconstruction. However, when faced with large data gaps in global grid datasets such as EMAG2, traditional interpolation approaches are often unable to effectively recover the missing information. In recent years, artificial intelligence methods have made breakthroughs in the reconstruction of sparse geomagnetic anomaly data [14–17]. For instance, Fangyuan Mao et al. [18] applied the diffusion model (RePaint) to reconstruct geomagnetic anomaly data. They generated the first complete high-resolution EMAG2 dataset, resolving the persistent data gap issue. Izham et al. [19] proposed a cVAE-GAN hybrid framework to reconstruct 1′ low-resolution geomagnetic data into 1″ high-resolution data. They also explicitly pointed out that this reconstruction recovers features, not the physically lost frequency components. Yiyang Li et al. [20] developed a reconstruction method that integrates spatially adaptive mean compensation with block-based sparse coding. The method better preserves both the low-frequency background and high-frequency details of geomagnetic data compared with traditional interpolation methods. Existing methods rely heavily on the spatial statistical relationships captured by limited measurements, primarily employing data-driven interpolation-based reconstruction frameworks to infer regions without measurements, and generally make limited use of the underlying physical properties of the geomagnetic field. When measurements are sparse or contain missing values, the reconstruction process is insufficiently constrained by the available data, making it prone to generating spurious artefacts that are inconsistent with the actual spatial distribution of the geomagnetic field, thereby compromising the accuracy and reliability of geomagnetic field model reconstruction. Furthermore, existing methods remain subject to limitations in terms of automation and computational efficiency, making them inadequate for the practical requirements of rapid geomagnetic field reconstruction over large marine areas and geomagnetic matching navigation for underwater applications.

On the other hand, existing marine geomagnetic field models are characterised by highly heterogeneous data sources. The data used for constructing marine geomagnetic

models are derived primarily from satellite, shipborne, and airborne magnetic surveys, which are highly complementary in terms of spatial coverage and resolution. Satellite data, being relatively far from the field sources, suffer from attenuation of small-scale magnetic anomalies. In contrast, shipborne and airborne magnetic surveys offer advantages in accuracy and resolution and represent important means of acquiring marine geomagnetic data. However, shipborne and airborne geomagnetic data over oceanic areas remain insufficient, with many regions still constituting survey gaps. Therefore, the practical application of underwater geomagnetic matching navigation calls for the development of effective multi-source data fusion methods to strengthen data-driven constraints, synergistically integrate information from multi-source information, and construct a geomagnetic field model with enhanced reconstruction accuracy.

Neural networks possess powerful capabilities for processing massive datasets and exhibit excellent approximation performance for highly complex nonlinear functions. They are characterised by parallel computing, distributed storage, fault tolerance, and strong learning ability. They can map various complex relationships in geophysical systems and fuse multi-source data to accomplish regression tasks with high accuracy and efficiency [21,22]. In recent years, neural networks have been successfully applied to bathymetric prediction [23–25], satellite gravity inversion [26,27], and geomagnetic interpolation [28,29]. Geomagnetic model data typically exist in the form of gridded files, whereas geomagnetic measurements originate from shipborne survey tracks, resulting in heterogeneous spatial data structures. As one of the classic neural network architectures, the fully connected neural network (FC-DNN) is simple in structure and performs well in terms of handling complex nonlinear problems. Therefore, we introduce the FC-DNN for multi-source marine geomagnetic data fusion.

This study proposes a multi-source data fusion method for the refined reconstruction of a marine geomagnetic field model based on a fully connected neural network architecture designated as MAG-DFN. The proposed approach uses the large-scale background field provided by the EMAG2 V3 geomagnetic model as a basis and incorporates the high-accuracy and high-resolution information contained in shipborne geomagnetic measurements. MAG-DFN is employed to learn the spatial differences between the background model and the measured geomagnetic field, thereby reconstructing the EMAG2 model and producing a high-accuracy geomagnetic field model for underwater geomagnetic navigation. On this basis, a residual learning strategy is introduced, in which the geomagnetic anomaly values from the background model and geographic coordinates are used as network inputs, while the differences between the shipborne measurements and the corresponding EMAG2 model values are defined as residuals and used as the supervisory signal. This enables the network to focus on learning local geomagnetic anomaly features that are difficult to represent using the EMAG2 model, thereby enhancing the representation of local magnetic field information while preserving the large-scale background field. To validate the effectiveness of the proposed approach, two study regions were selected, where a subset of the shipborne measurements was used to train the network, and the trained network was subsequently applied to reconstruct the geomagnetic field model. Meanwhile, the measurements excluded from the training process were retained as an independent validation dataset, thereby forming blank areas where no shipborne measurements were used for training. The accuracy and reliability of the proposed approach were evaluated by comparing the reconstructed model in the blank areas with both the EMAG2 model and the corresponding shipborne measurements.

2. Study Area and Data

2.1. Study Area

The South China Sea is located at the junction of the Eurasian, Indo-Australian, and Philippine Sea plates, forming part of the western Pacific marginal sea system. As one of the largest marginal seas in the world, its formation and evolution represent a frontier topic in Earth sciences, and it provides a natural geological laboratory for the study of continental rifting and seafloor spreading processes. The area of the South China Sea and the adjacent western Pacific is rich in diverse tectonic units, including trenches, basins, and submarine plateaus, and characterised by numerous seamounts, islands, and complex seafloor topography. With considerable topographic relief, this marine area generates distinctive gravity and geomagnetic field signatures. The marine geomagnetic field of the South China Sea and the adjacent western Pacific serves as fundamental data for studying crustal structure and tectonic units, while its complex spatial characteristics offer an ideal testbed for validating the performance of the MAG-DFN method. Therefore, we select two sub-areas within the South China Sea and the western Pacific Ocean as the study areas. The two study areas, each measuring 4° × 8°, are Area A (17–21° N, 112–120° E) and Area B (20–24° N, 122–130° E).

2.2. EMAG2v3 Model

In this study, the sea-level version of EMAG2v3 (Earth Magnetic Anomaly Grid at 2 arc min Resolution Version 3) is adopted as the background geomagnetic field model. EMAG2v3 was released by Meyer et al. in 2017. Compared with the earlier EMAG2, it is compiled without any a priori information on geological structures or ocean-floor age, relying solely on observed data; therefore, it provides a more realistic representation of the complex magnetic anomaly patterns along oceanic spreading ridges and continental margins [8].

Different main-field models were used for data reduction depending on the epoch: data collected before 1962 were corrected only for the core field using IGRF; data from 1962 to 1999 were corrected for both core and external fields using CM4; and data from 2000 onward were corrected for the core field using CHAOS-5 and for external fields using CM4. To accurately represent anomalies with wavelengths greater than 300 km, EMAG2v3 incorporates the satellite-derived lithospheric field model MF7 and merges it with observed data through spherical harmonic inversion. In addition, EMAG2v3 provides a global error distribution map in its official quality-report paper, with a total error of approximately 100 nT in oceanic regions and about 128 nT in the South China Sea and western Pacific. Figure 1 shows the sea-level magnetic anomaly distribution of EMAG2v3 over the two study areas.

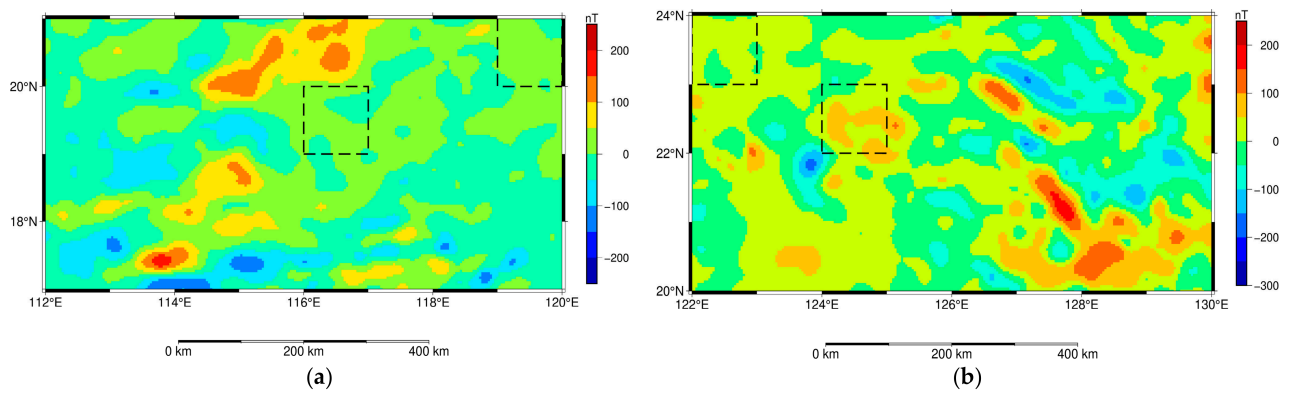


Figure 1. EMAG2v3 magnetic anomaly maps of two study areas. The dotted rectangles represent the validation areas. (**a**) Area A; (**b**) Area B.

2.3. Shipborne Measurements

Shipborne magnetic measurements can effectively determine geomagnetic anomalies along survey tracks, and they achieve high accuracy and reliability in the intermediate-to-short wavelength band (approximately 10–200 km), making them a core data source for high-resolution marine magnetic anomaly modelling. This study uses publicly available shipborne geomagnetic anomaly measurements provided by the National Marine Data Center, National Science & Technology Resource Sharing Service Platform of China [30]. This dataset is not incorporated into the EMAG2v3 global geomagnetic anomaly model. The shipborne data have already undergone position and attitude correction, diurnal correction, and main-field correction.

In the two study areas, 36 and 38 survey tracks were selected, initially containing 91,878 and 44,429 measurement points, respectively. The data were acquired between 1960 and 2011. The shipborne measurements were collected by different countries and institutions over several decades; the tracks differ in navigation accuracy and instrument performance, resulting in a certain degree of inconsistency among tracks [31], necessitating quality control. Because data from different periods used different IGRF main-field models and epochs, the survey tracks were grouped by acquisition year to reduce epoch-related differences, and crossover misfits were systematically calculated within each group [32,33]. On this basis, we perform both single-track self-assessment and multi-track cross-evaluation to support data screening and quality control. First, using each individual track as the basic unit, we compute the discrepancies in geomagnetic anomaly observations at all crossover points within the track. This allows us to remove segments of poor data quality to ensure the internal consistency and stability of the track itself. Subsequently, based on the self-assessment, we conduct a statistical analysis of the crossover network formed by multiple tracks. This enables us to effectively identify and remove anomalous tracks that exhibit poor consistency with the overall dataset, thereby mitigating systematic errors and ensuring the coherence of the entire dataset. After quality control, the crossover-misfit STD in Area A decreased from 21.50 nT to 13.61 nT, with 7.35% of the data points removed. In Area B, the STD decreased from 10.79 nT to 6.64 nT, with 8.63% of the data points removed. Detailed data are shown in Table 1. These results indicate that the quality-control procedure effectively reduced the inconsistency among the tracks. Finally, because of the inconsistent reference bases, a systematic difference exists between the shipborne measurements and EMAG2v3, and the shipborne data need to be aligned to the EMAG2v3 reference. Since the study area is relatively small, the difference in reference bases is approximately constant within the region, and a constant bias correction is therefore adopted to remove the systematic difference. It should be noted that this step only applies a constant shift to the shipborne data and does not alter the spatial pattern or relative amplitudes of the anomalies, thus preserving the key information required for matching navigation.

Table 1. Statistics of crossover misfit before and after quality control for Area A and Area B.

Area	QC Status	Number of Tracks	Number of Points	STD (nT)
A	Before	36	91,878	21.50
	After	29	85,126	13.61
B	Before	38	44,429	10.79
	After	37	40,394	6.64

To provide a more robust evaluation of spatial generalisation, two 1° × 1° blocks are selected as withheld validation areas in each study area: the corner blocks are designated

A-1 and B-1, and the interior blocks are designated A-2 and B-2. After quality control, 85,126 points in Area A and 40,394 points in Area B are retained for subsequent computation. For block A-1, 82,715 points are used for training and 2411 points are used for validation; for block A-2, 83,824 points are used for training and 1302 points are used for validation. Similarly, for block B-1, 35,824 points are used for training and 4570 points are used for validation; for block B-2, 40,174 points are used for training and 220 points are used for validation. Their distribution is shown in Figure 2.

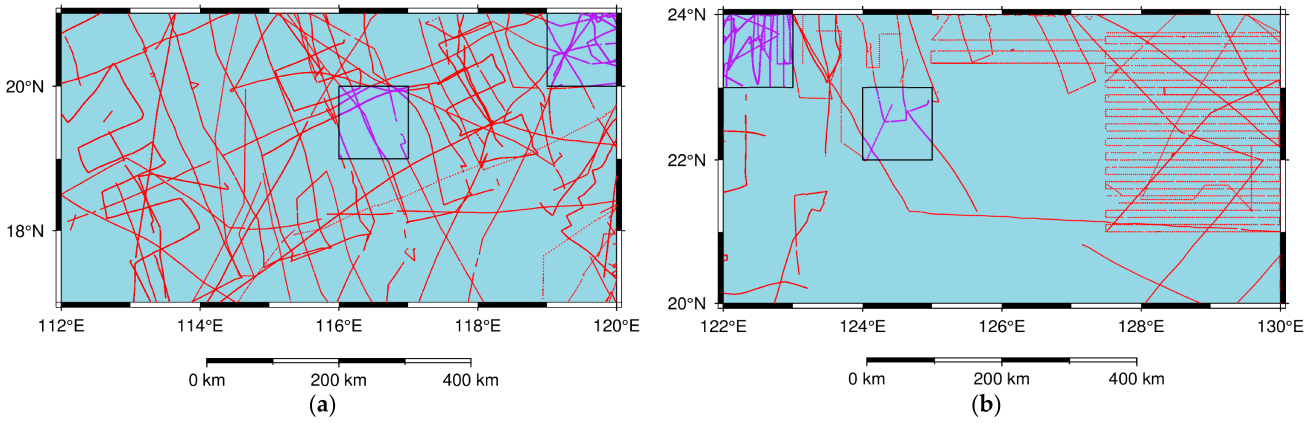


Figure 2. The distribution of the training and validation data. Red lines and purple lines represent training data and validation data, respectively. (**a**) Area A; (**b**) Area B.

3. Methodology

In this study, the MAG-DFN approach is applied to reconstruct the EMAG2 V3 model using corrected high-accuracy marine shipborne geomagnetic measurements. The overall technical workflow is illustrated in Figure 3.

The main procedure is summarised as follows. First, the acquired geomagnetic measurements are subjected to quality control and preprocessing to ensure the reliability of the data used in the experiment. Based on this, geomagnetic model residuals are constructed from the differences between the geomagnetic anomalies obtained from the measurements and the corresponding values from the EMAG2v3. MAG-DFN is then employed to learn the nonlinear relationship between the geomagnetic residuals, spatial locations, and the background model, thereby obtaining the predicted residuals within the study area. The predicted residuals are subsequently added to the EMAG2 background model to obtain the final reconstructed geomagnetic model, designated FN_MAG.

3.1. MAG-DFN: A Fully Connected Neural Network Method for Local Marine Geomagnetic Anomaly Model Reconstruction

Existing methods for marine geomagnetic field reconstruction rely primarily on the spatial statistical relationships within limited measurements. In data-sparse or measurement-deficient regions, insufficient effective constraints can lead to substantial reconstruction errors, while their ability to characterise local magnetic anomalies is also limited. Meanwhile, geomagnetic data from different sources exhibit clear complementarity in terms of spatial coverage, accuracy, and resolution. A single data source or a simple data fusion strategy is insufficient to simultaneously capture the large-scale background field and local fine-scale structures. Moreover, directly superimposing multi-source data or combining them through conventional interpolation methods cannot fully exploit the complementary strengths of different data sources. How to effectively exploit multi-source geomagnetic information and the background-field constraints provided by existing models to improve

the accuracy and reliability of geomagnetic field reconstruction under conditions of limited measurements remains an open issue requiring further investigation.

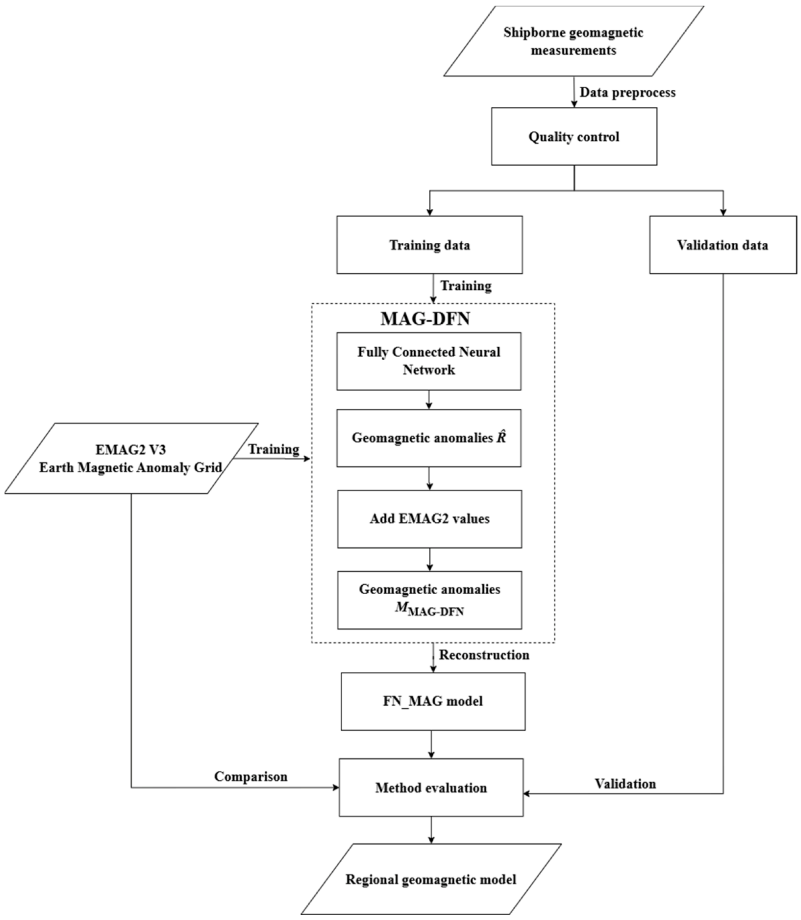


Figure 3. Workflow of the proposed approach.

To address the aforementioned issues, this study proposes MAG-DFN, a fully connected neural network method for local marine geomagnetic anomaly model reconstruction via multi-source data fusion. From the perspective of multi-source information fusion, the proposed approach uses the EMAG2 geomagnetic model as the large-scale background field and shipborne geomagnetic measurements as local high-accuracy constraints. MAG-DFN adopts a residual learning strategy, in which the differences between the EMAG2 geomagnetic model and the measurements are taken as the primary learning target, and the geomagnetic field model is refined by learning the model residuals. The geographic position of a given point is denoted by longitude *Lon* and latitude *Lat*. The geomagnetic anomaly obtained from shipborne measurements at this point is denoted by M_{obs}, while the corresponding geomagnetic anomaly value from the EMAG2 model is denoted by M_{EMAG2}. The geomagnetic model residual at this point is therefore defined as follows:

$$R = M_{\mathrm{obs}} - M_{\mathrm{EMAG2}}, \tag{1}$$

where R represents the local residual between the EMAG2 background model and the geomagnetic field at the given location. Its magnitude reflects the local geomagnetic anomaly information that is not adequately represented by the EMAG2 model at that location.

Therefore, the core of MAG-DFN is not to relearn the entire geomagnetic field but to learn the regional-scale discrepancies and spatial details that are not adequately represented by the existing model. This strategy enables the large-scale field information provided by

the background model and the local correction information contained in the shipborne measurements to be jointly exploited, thereby avoiding direct remodelling of the complete geomagnetic field and reducing the learning difficulty associated with predicting the entire field directly. While preserving the large-scale geomagnetic field characteristics of the background model, MAG-DFN further incorporates the fine-scale information contained in the shipborne measurements, providing stable prior constraints for model reconstruction. In this way, the discrepancies and missing spatial details of the background model can be compensated for, thereby enhancing its capability to represent local geomagnetic anomalies.

To further enhance the model's capability to characterise the spatial distribution of the geomagnetic field, geographic location information is incorporated into the MAG-DFN framework as auxiliary input features. By incorporating geographic spatial information, a nonlinear mapping relationship is established between the residuals and spatial location, enabling the network to automatically learn the spatial distribution characteristics of geomagnetic field residuals and effectively capture their spatial dependencies and variations, thereby reducing reliance on conventional manual interpolation and empirically determined parameter settings. The overall architecture of MAG-DFN for the refined reconstruction of the geomagnetic field models is illustrated in Figure 4.

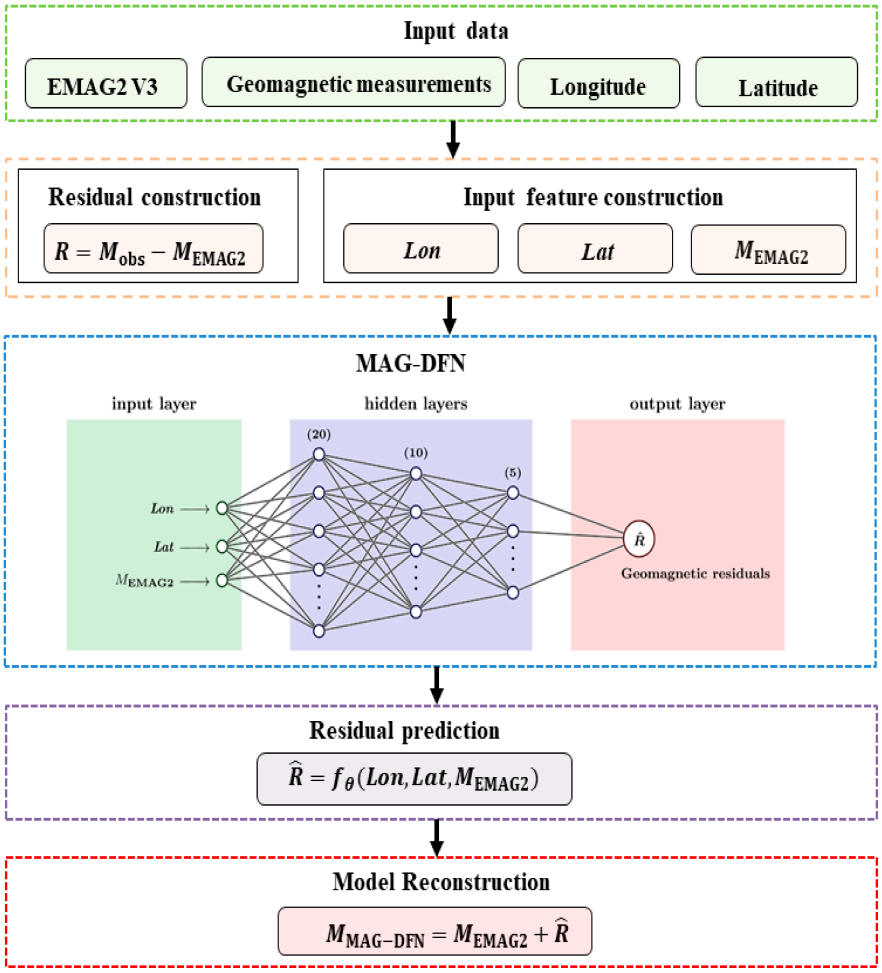


Figure 4. Schematic diagram of the MAG-DFN architecture for refined reconstruction of marine geomagnetic field models.

MAG-DFN employs a fully connected network as its core architecture. The input layer consists of three feature components, namely longitude, latitude, and the geomagnetic anomaly value from the EMAG2 model. The input feature vector is given by the following:

$$x = [Lon, Lat, M_{\mathrm{EMAG2}}]^{\mathrm{T}}. \quad (2)$$

The output feature is the geomagnetic field residual R, while the residual supervisory signal is derived from the shipborne measurements to train the network to learn the spatial distribution of the residuals.

The network performs successive nonlinear mappings of the input features through the hidden layers to learn the complex relationships among geographic location, the background geomagnetic field, and the geomagnetic field residual. After extensive tuning and comparative analysis, the hidden layers were ultimately configured as three fully connected layers with 20, 10, and 5 neurons, respectively. Each neuron performs feature extraction and nonlinear transformation on the input data through specific mathematical operations. Neurons between adjacent layers are fully connected via learnable weight parameters. The forward propagation process can be formalised as Equations (3) and (4).

$$R = W_4\sigma(W_3\sigma(W_2\sigma(W_1x + b_1) + b_2) + b_3) + b_4, \quad (3)$$

$$\sigma(z) = \max(0, z). \quad (4)$$

where W represents the four layer weight matrices, b represents the three layer bias vectors, and σ represents the activation function. The activation function enhances the feature representation capability of the network by introducing nonlinear transformations, enabling it to model the complex nonlinear relationships between the input features and the geomagnetic field residual. In this study, the ReLU function is employed as the activation function in the hidden layers to enhance the nonlinear representation capability of the network and improve the efficiency of gradient propagation during the training of the network. The output layer uses a linear activation function so that the predicted residual can take both positive and negative values. Through the configuration of these layers, the model is able to learn the complex nonlinear relationship between geographic location and geomagnetic field information, thereby enabling the accurate prediction of geomagnetic anomalies.

The network parameters are iteratively optimised through backpropagation. In this study, the mean squared error (MSE) is adopted as the loss function during the training stage to quantify the difference between the predicted residuals and the true residuals. The root mean squared error (RMSE) is additionally employed to evaluate the predictive performance of the model. The network parameters are updated using the Adam optimisation algorithm, and the parameter update process is expressed in Equation (5).

$$\theta^{(t+1)} = \theta^{(t)} - \eta\frac{\hat{m}_t}{\sqrt{\hat{v}_t} + \varepsilon}, \quad (5)$$

where θ represents the weights (W) and biases (b), η represents the learning rate, and $\hat{m}_t$ and $\hat{v}_t$ represent the bias-corrected estimates of the first and second moments of the gradients, respectively. In this study, the initial learning rate was $\eta = 0.001$, with $\beta_1 = 0.9$, $\beta_2 = 0.999$, and $\varepsilon = 1 \times 10^{-7}$, where β_1 and β_2 are the exponential decay rates for the first and second moment estimates, and ε is a small stabiliser constant used to prevent division by zero. Adam is a first-order gradient-based stochastic optimisation algorithm that adaptively adjusts the parameter update steps according to historical gradient information, thereby improving the stability and convergence efficiency of network training. These procedures are primarily used to adjust the weights of the neural network. The weights and biases are assigned initial values during network initialisation, and the weights of individual neurons are updated according to the errors between the predicted and true residuals during training, thereby iteratively refining the performance of the network.

3.2. Training the Network and Prediction

Once the network architecture is established, model training and prediction are conducted as follows.

First, the three input features are arranged according to their corresponding spatial locations to form a two-dimensional input matrix, which is then used as the input tensor. Meanwhile, the geomagnetic field residuals are calculated from the measurements and the corresponding EMAG2 model values, with the difference between them used as the supervisory labels for network training. In addition, because different input features vary in numerical ranges and units, directly feeding them into the network may result in imbalanced contributions to model training. Therefore, the StandardScaler is employed to normalise the data. The StandardScaler was fitted on the training data only and then applied to the validation and test sets, so that no information from the validation or test data was used during normalisation. Normalisation eliminates the effects of different feature scales and numerical ranges, improves the comparability among features, and contributes to the stability and convergence speed of network training.

Second, the weights are initialised using the default Glorot uniform initialiser in Keras, with the biases initialised to zero. To assess the stability of the results with respect to random initialisation, each experiment was repeated 5 times using random seeds 1–5. The normalised input data are fed into the network and propagated forward through the hidden layers, ultimately producing the normalised predicted geomagnetic residuals.

Third, the error between the predicted output and the target value is calculated. When the error exceeds the expected threshold, it is propagated back through the network. Subsequently, backpropagation is employed to calculate the gradients of the loss function with respect to the network parameters. The Adam optimiser adaptively updates the network weights and biases based on the first and second moments of the gradients. Through multiple iterations, the loss function gradually converges, completing the model training process. In this study, after extensive tuning, the network was trained for 80 epochs with a batch size of 128 and an initial learning rate of 0.001. The training data were randomly split into a training subset (80%) and an inner validation subset (20%), and the validation loss was computed on this inner subset. The withheld blank-area data were kept separate and used only for the final independent evaluation. The ReduceLROnPlateau callback was configured with a patience of 3 epochs, a decay factor of 0.5, a minimum learning rate of 1×10^{-7}, and a cooldown of 1 epoch. An early-stopping criterion was applied with a patience of 20 epochs, restoring the best weights at the end of training. When the validation loss failed to improve over consecutive epochs, the learning rate was reduced to 50% of its current value. The model was implemented in TensorFlow 2.21.0 with Keras 3.15.0, and the data preprocessing was performed using scikit-learn 1.6.1 (NumPy 2.1.3).

Finally, for any grid point within the study area, the longitude, latitude, and EMAG2v3 geomagnetic anomaly value at that location are scaled using the same scalers that were fitted on the training data and then input into the trained network to obtain the corresponding normalised geomagnetic field residual prediction. Subsequently, the predicted residuals are transformed back to the original units using the inverse transformation and added to the corresponding EMAG2v3 values to obtain the geomagnetic anomalies. For grid nodes outside the training range, the scaled values are allowed to exceed the range $[0, 1]$. After applying the above procedure to all grid points within the study area, the reconstructed results are reorganised according to their spatial locations to generate the final FN_MAG geomagnetic model.

4. Results and Evaluation

4.1. Reconstructed FN_MAG Model

The FN_MAG geomagnetic anomaly model for the study region was reconstructed from the EMAG2 model using the MAG-DFN approach, as shown in Figure 5. For each study region, the best-performing run among the five repeated runs (lowest validation RMSE, together with its corresponding withheld validation block) was selected to generate the final FN_MAG product. All geomagnetic anomaly maps presented in this study are referenced to sea level, and no upward or downward continuation has been applied. They are intended for sea-level interpretation only and should not be used directly for subsurface interpretation without accounting for the increase in field amplitude with depth.

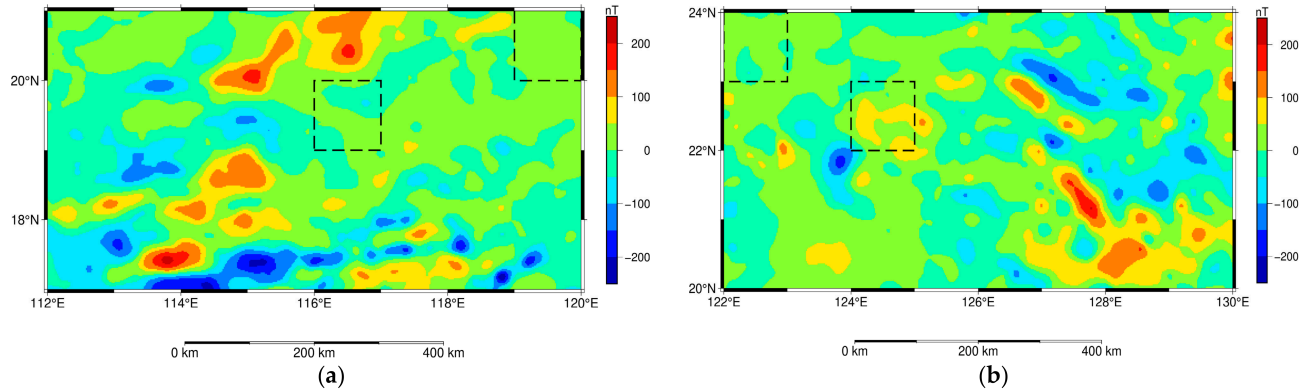


Figure 5. Reconstructed FN_MAG geomagnetic anomaly model for two study areas. (**a**) Area A; (**b**) Area B.

Furthermore, to enable a direct comparison between FN_MAG and EMAG2, we calculate the prediction residual (FN_MAG-EMAG2) and plot its distribution to observe local-scale detailed differences in FN_MAG relative to EMAG2, as shown in Figure 6. Positive values indicate that FN_MAG increases the anomaly relative to EMAG2, while negative values indicate a decrease.

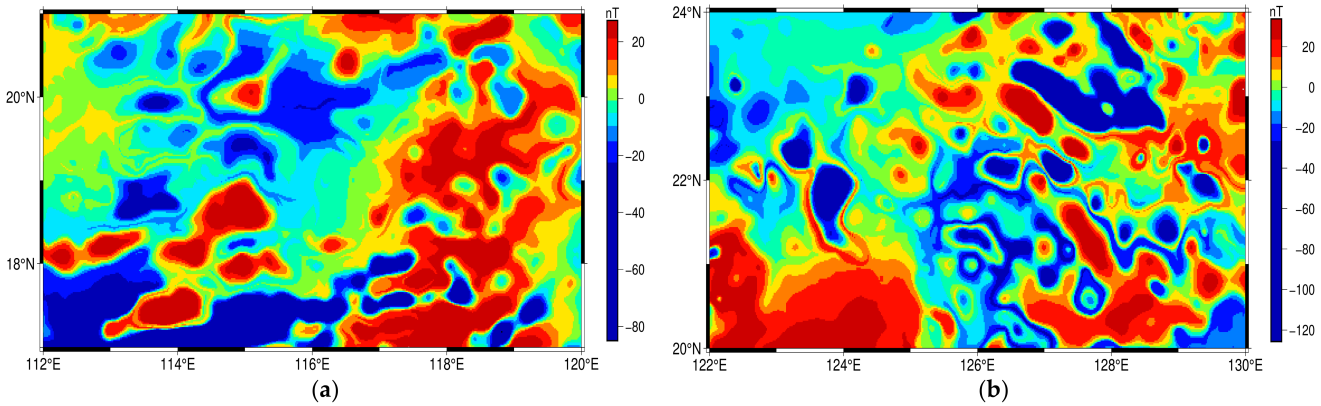


Figure 6. Distribution of the prediction residual (FN_MAG-EMAG2) in two study areas. (**a**) Area A; (**b**) Area B.

4.2. Method Evaluation

To assess the stability of the results with respect to random initialisation, each experiment was repeated five times using random seeds 1–5, and the results are reported as mean ± standard deviation over the five runs. To further evaluate whether the improvement in MAG-DFN goes beyond a simple bias correction, FN_MAG was compared with EMAG2 and

four baseline methods, including constant bias removal (Bias-removed), Kriging, Gaussian-process regression (GPR), and random forest. All baseline models were trained using the same shipborne measurements and residual targets as MAG-DFN, and their performances were evaluated on the identical independent validation dataset. All methods were evaluated on exactly the same withheld validation points. EMAG2 and the baseline methods are deterministic and are reported as single values. We calculated the statistical metrics of all methods, including the arithmetic mean (mean), the mean absolute error (MAE), the root mean square error (RMSE), the standard deviation of the differences (STD), and the concordance correlation coefficient (CCC), covering the results of FN_MAG, EMAG2, and the four baseline methods relative to the shipborne measurements, as presented in Table 2.

Table 2. Statistical evaluation of FN_MAG, EMAG2, and four baseline methods relative to shipborne geomagnetic measurements.

Area	Data	Min (nT)	Max (nT)	Mean (nT)	MAE (nT)	RMSE (nT)	STD (nT)	CCC
A-1	FN_MAG vs. ship	−96.07 ± 1.0	116.85 ± 0.7	10.74 ± 0.4	22.85 ± 0.18	29.65 ± 0.14	27.03 ± 0.14	0.446 ± 0.01
	EMAG2 vs. ship	−87.63	124.37	18.71	26.79	33.11	27.31	0.301
	Bias-removed vs. ship	−87.16	123.49	18.36	26.62	32.95	27.37	0.381
	Kriging vs. ship	−97.45	118.33	2.71	25.62	31.20	29.65	0.340
	GPR vs. ship	−153.36	126.83	7.37	27.55	37.64	37.54	0.014
	Random forest vs. ship	−142.40	109.35	5.20	31.08	39.11	38.76	0.012
A-2	FN_MAG vs. ship	−75.06 ± 0.9	76.82 ± 0.9	−13.24 ± 0.8	24.75 ± 0.57	31.06 ± 0.66	25.45 ± 0.15	0.478 ± 0.02
	EMAG2 vs. ship	79.13	61.73	−26.43	31.31	38.21	27.59	0.216
	Bias-removed vs. ship	−80.00	60.86	−27.03	31.82	38.82	28.19	0.212
	Kriging vs. ship	−102.02	40.33	−26.15	28.63	46.64	28.83	0.071
	GPR vs. ship	−78.27	62.59	−27.08	32.18	39.15	28.26	0.215
	Random forest vs. ship	−107.03	52.51	−35.78	39.56	47.22	30.82	0.169
B-1	FN_MAG vs. ship	−103.05 ± 1.0	111.89 ± 1.2	3.54 ± 0.9	23.80 ± 0.10	31.91 ± 0.11	30.95 ± 0.07	0.395 ± 0.003
	EMAG2 vs. ship	−132.23	83.97	−20.58	29.52	37.23	31.05	0.205
	Bias-removed vs. ship	−139.95	160.71	−10.64	28.83	36.79	34.74	0.0004
	Kriging vs. ship	−138.22	72.94	−26.01	33.47	41.42	32.23	0.125
	GPR vs. ship	−166.15	94.10	−9.26	28.31	38.31	37.18	0.082
	Random forest vs. ship	−133.05	98.68	−24.16	34.67	43.14	35.75	0.024
B-2	FN_MAG vs. ship	−130.22 ± 2.0	148.90 ± 0.9	−11.82 ± 0.6	44.86 ± 0.15	55.68 ± 0.21	53.91 ± 0.16	0.449 ± 0.003
	EMAG2 vs. ship	−125.13	148.09	−11.83	48.33	58.92	54.73	0.305
	Bias-removed vs. ship	−253.73	287.18	−7.43	57.23	71.44	71.06	0.002
	Kriging vs. ship	−118.93	157.81	−3.33	45.25	55.31	55.21	0.357
	GPR vs. ship	−129.49	143.61	−15.61	47.17	57.25	55.62	0.352
	Random forest vs. ship	−247.58	77.72	−58.43	72.76	89.79	68.17	0.183

As shown in Table 2, FN_MAG achieves the lowest RMSE in all four validation blocks. Compared with EMAG2, FN_MAG reduces the MAE by 14.71%, 23.35%, 22.09%, and 8.96% and the RMSE by 12.41%, 18.87%, 16.73%, and 6.65% in blocks A-1, A-2, B-1, and B-2, respectively, indicating a higher agreement with the shipborne measurements. Meanwhile, compared with the four baseline methods, MAG-DFN achieves relatively superior performance in the validation region, which suggests that the model possesses a reasonably promising spatial extrapolation capability.

To make the comparison more directly interpretable, the shipborne values are compared with the EMAG2 and FN_MAG estimates at the same ship-track locations in the blank areas of the two study areas, as shown in Figure 7.

Additionally, to evaluate the contribution of each input feature to the prediction, an input ablation study was performed by comparing two input configurations, namely longitude and latitude only, and all three inputs. Both configurations used the same network architecture, training settings, and random seed (the one with the lowest validation RMSE) and were evaluated on the same withheld validation points. The statistical results are summarised in Table 3.

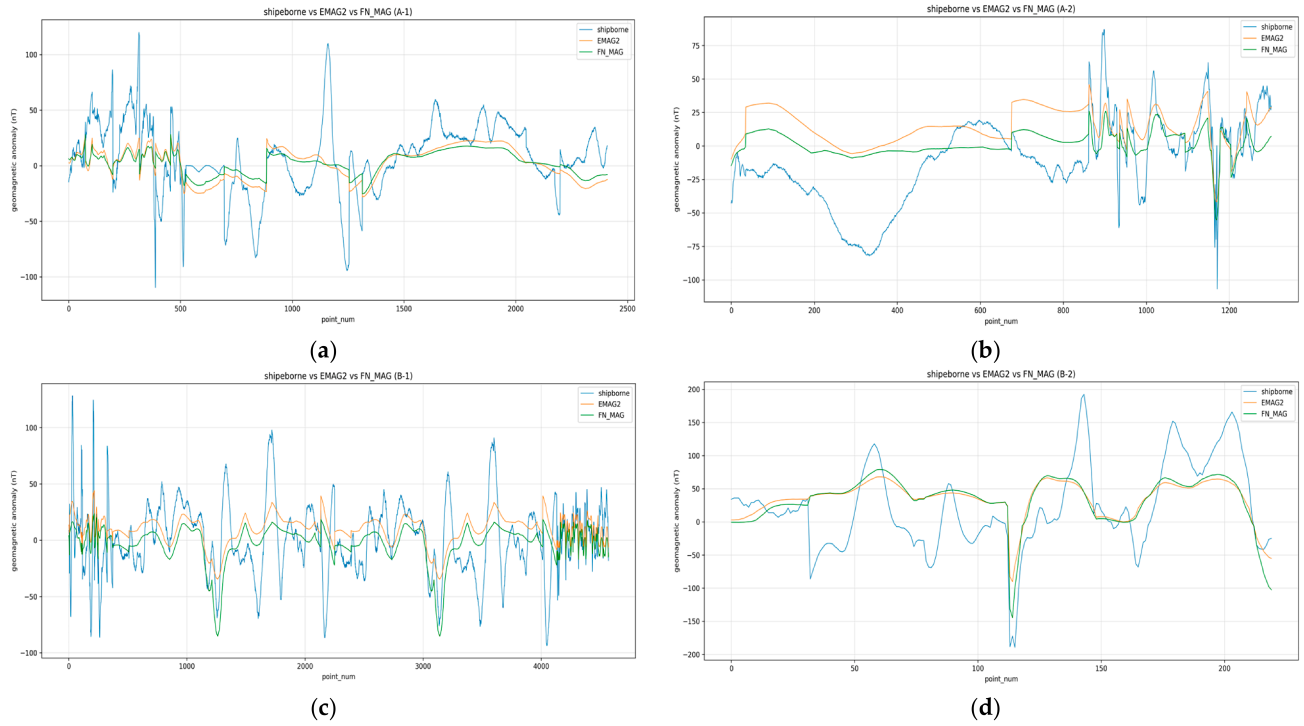


Figure 7. Comparison of the shipborne geomagnetic anomalies with the EMAG2 and FN_MAG estimates along the ship tracks in four validation areas. Blue: shipborne measurements; orange: EMAG2; green: FN_MAG. (**a**) A-1; (**b**) A-2; (**c**) B-1; (**d**) B-2.

Table 3. Comparison of different input configurations in the input ablation study.

Region	Input Configuration	Min (nT)	Max (nT)	Mean (nT)	MAE (nT)	RMSE (nT)	STD (nT)	CCC
A-1	Lon/Lat	−106.36	170.25	28.02	41.19	50.18	41.63	0.044
	Lon/Lat/EMAG2	−97.37	115.02	10.32	22.66	29.52	27.03	0.437
A-2	Lon/Lat	−323.65	179.93	19.46	86.44	102.86	101.01	0.107
	Lon/Lat/EMAG2	−73.85	77.82	−12.04	23.91	30.06	25.23	0.588
B-1	Lon/Lat	−167.04	155.85	−11.56	30.49	43.46	41.89	0.053
	Lon/Lat/EMAG2	−103.48	110.29	3.14	23.21	31.81	30.75	0.407
B-2	Lon/Lat	−264.44	96.56	−26.42	59.52	80.10	75.61	0.033
	Lon/Lat/EMAG2	−129.72	149.67	−11.64	44.56	55.26	53.57	0.456

As presented in Table 3, adding the EMAG2 anomaly value as an additional input substantially improves the prediction in all four validation blocks. The RMSE decreases by 42.21%, 70.82%, 28.67%, and 31.34% in blocks A-1, A-2, B-1, and B-2, respectively, and the MAE decreases by 46.59%, 72.24%, 24.57%, and 26.08%. These results confirm that the EMAG2 background value provides essential information for predicting the local residuals, and that the network does not rely on geographic location alone.

In summary, the baseline comparison confirms that MAG-DFN outperforms EMAG2 and all baseline methods across the validation blocks, demonstrating that the improvement is not merely a bias correction but reflects the ability of the network to capture local anomaly structure. The input ablation study further shows that the EMAG2 background value is an essential input, as removing it leads to a substantial degradation in prediction performance. Taken together, these results indicate that MAG-DFN effectively exploits the

EMAG2 background information while learning the local anomaly features that EMAG2 does not represent, thereby better supporting matching navigation applications.

5. Conclusions

This study proposes a local marine geomagnetic anomaly model reconstruction approach via multi-source data fusion based on a fully connected neural network. The proposed MAG-DFN method takes the EMAG2 model as the prior background field input, while shipborne geomagnetic measurements are used to construct the residual supervision information. Through residual learning, these two types of information are effectively integrated to reconstruct the EMAG2 model. To evaluate the performance of the proposed approach, two sub-areas in the South China Sea and the western Pacific were selected for experiments, and two 1° × 1° validation blocks were withheld in each area to assess spatial generalisation. In addition, four baseline methods were introduced for comparison.

The results show that FN_MAG consistently outperforms EMAG2 and all baseline methods across the validation blocks. Compared with EMAG2, FN_MAG substantially reduces both the MAE and RMSE and achieves a much higher concordance correlation coefficient with the shipborne measurements. More importantly, relative to four baselines, FN_MAG further reduces the MAE and RMSE, confirming that the improvement goes beyond a simple bias correction and that the network captures a local anomaly structure that EMAG2 does not represent. The input ablation study further demonstrates that the EMAG2 background value is an essential input, as removing it leads to a marked degradation in prediction performance.

Overall, the proposed method combines the large-scale background field of EMAG2 with shipborne measurements, and the improved agreement with the shipborne data suggests that the network captures part of the local anomaly information that EMAG2 does not represent. These results suggest that MAG-DFN has potential value for matching navigation applications and provides a useful reference for future marine geomagnetic modelling.

Author Contributions: M.W., L.W. and Z.P. conceived this study and designed the experiments. M.W. and L.W. carried out the experiments and wrote the initial draft of the manuscript. Z.P., S.L., Q.L., L.B., and Y.W. analysed the results and revised the manuscript. All authors have read and agreed to the published version of the manuscript.

Funding: This work was supported by the National Natural Science Foundation of China (Grant Nos. 42274116, 42404004), Hainan Province Science and Technology Special Fund (Grant No. ZDYF2024SHFZ086), the Independent Project of State Key Laboratory of Precision Geodesy, Innovation Academy for Precision Measurement Science and Technology, Chinese Academy of Sciences (Grant No. ZD202501), Central Government Funds for Hubei Science & Technology Development (Grant No. 2025CSA009), and the Natural Science Foundation of Wuhan (Grant No. 2024040701010065).

Institutional Review Board Statement: Not applicable.

Informed Consent Statement: Not applicable.

Data Availability Statement: The data that support the findings of this study are available from the corresponding author upon reasonable request.

Acknowledgments: We acknowledge the National Science and Technology Resource Sharing Service Platform of China—National Marine Science Data Center (https://mds.nmdis.org.cn/) for providing support with the data used in this study, accessed on 15 November 2025. The NOAA (National Oceanic and Atmospheric Administration) National Centers for Environmental Information (NCEI) provided the Earth Magnetic Anomaly Grid EMAG2 v3, which is available at https://www.ncei.noaa.gov/products/earth-magnetic-model-anomaly-grid-2, accessed on 22 October 2024.

Conflicts of Interest: The authors declare no conflicts of interest.

References

1. Chen, Z.; Zhang, X.; Li, Y.A. New Geomagnetic matching navigation method based on multidimensional vector elements of Earth's magnetic field. *IEEE Geosci. Remote Sens. Lett.* **2018**, *15*, 1289–1293. [CrossRef]
2. Lu, Y.; Wei, D.Y.; Ji, X.C.; Yuan, H. Review of geomagnetic positioning methods. *Navig. Position. Timing* **2022**, *2*, 118–130.
3. Dinc, M.; Hajiyev, C. Integration of navigation systems for autonomous underwater vehicles. *J. Mar. Eng. Technol.* **2015**, *14*, 32–43. [CrossRef]
4. Canciani, A.; Raquet, J. Absolute positioning using the Earth's magnetic anomaly field. *Navigation* **2016**, *63*, 111–126. [CrossRef]
5. Wardinski, I.; Saturnino, D.; Amit, H.; Chambodut, A.; Langlais, B.; Mandea, M.; Thébault, E. Geomagnetic core field models and secular variation forecasts for the 13th International Geomagnetic Reference Field (IGRF-13). *Earth Planets Space* **2020**, *72*, 155. [CrossRef]
6. Firsov, I.; Kudin, D.; Soloviev, A.; Krasnoperov, R.; Dobrovolsky, M. GCRAS candidate field models for IGRF-14. *Earth Planets Space* **2026**, *78*, 9. [CrossRef]
7. Yao, H.; Liu, P.; Yan, Q.; Jiang, Y.; Xu, J.; Yin, L.; Ren, Z.; Lin, Y.; Feng, Y.; Pan, Y.; et al. MISTA candidate magnetic field models for IGRF-14 derived from MSS 1, Swarm and observatory data. *Earth Planets Space* **2025**, *77*, 184. [CrossRef]
8. Meyer, B.; Chulliat, A.; Saltus, R. Derivation and error analysis of the Earth Magnetic Anomaly Grid at 2 arc min Resolution Version 3 (EMAG2v3). *Geochem. Geophys. Geosyst.* **2017**, *18*, 4522–4537. [CrossRef]
9. Maus, S.; Barckhausen, U.; Berkenbosch, H.; Bournas, N.; Brozena, J.; Childers, V.; Dostaler, F.; Fairhead, J.D.; Finn, C.; von Frese, R.R.B.; et al. EMAG2: A 2-arc min resolution Earth Magnetic Anomaly Grid compiled from satellite, airborne, and marine magnetic measurements. *Geochem. Geophys. Geosyst.* **2009**, *10*, Q08005. [CrossRef]
10. Jiao, L.; Tu, J.; Lei, Y.; Zhao, J.; Wang, W. Crustal magnetic structure and implications for the Eastern Himalayan Syntaxis revealed by EMAG2 v3. *Tectonophysics* **2025**, *896*, 230608. [CrossRef]
11. Li, H.; Zhang, Q.; Pan, M.; Chen, D.; Liu, Z.; Yan, L.; Xu, Y.; Ding, Z.; Yu, Z.; Liu, X.; et al. Accounting for geometric anisotropy in sparse magnetic data using a modified interpolation algorithm. *Remote Sens.* **2024**, *16*, 883. [CrossRef]
12. Niaraq, S.M.; Shahsavani, H. Fractal modeling of Baba Ali iron ore deposit geophysical data in western Iran for magnetic anomaly separation in GIS environment. *Sci. Rep.* **2025**, *15*, 42949. [CrossRef] [PubMed]
13. Lee, D.; Cho, H.; Kim, J. Spatiotemporal geomagnetic intensity mapping using Gaussian process for underwater vehicle localization. *J. Ocean Eng. Technol.* **2026**, *40*, 227–237. [CrossRef]
14. Datta, A.; Banerjee, S.; Finley, A.O.; Gelfand, A.E. On Nearest-Neighbor Gaussian Process Models for Massive Spatial Data. *WIREs Comput. Stat.* **2016**, *8*, 162–171. [CrossRef] [PubMed]
15. Dearmon, J.; Smith, T.E. A Hierarchical Approach to Scalable Gaussian Process Regression for Spatial Data. *J. Spat. Econom.* **2021**, *2*, 12. [CrossRef]
16. Hengl, T.; Nussbaum, M.; Wright, M.N.; Heuvelink, G.B.M.; Gräler, B. Random Forest as a Generic Framework for Predictive Modeling of Spatial and Spatio-Temporal Variables. *PeerJ* **2018**, *6*, e5518. [CrossRef] [PubMed]
17. Rodriguez-Galiano, V.; Sanchez-Castillo, M.; Chica-Olmo, M.; Chica-Rivas, M. Machine Learning Predictive Models for Mineral Prospectivity: An Evaluation of Neural Networks, Random Forest, Regression Trees and Support Vector Machines. *Ore Geol. Rev.* **2015**, *71*, 804–818. [CrossRef]
18. Mao, F.Y.; Yang, B.; Jin, S. Recovering missing regions of Earth Magnetic Anomaly Grid data (EMAG2) using RePaint based on diffusion model. *Big Data Earth Syst.* **2025**, *1*, 100004. [CrossRef]
19. Syahiran Izham, M.A.; Yusof, K.A.; Mohd Haniff, N.S.; Mashohor, S.; Abd Rahman, M.A.; Abdullah, M. CVAE GAN & STFT CNN for low resolution geomagnetic data reconstruction in Pi2 pulsation identification. *Adv. Space Res.* **2026**, *77*, 6315–6331. [CrossRef]
20. Li, Y.; Zhao, D.; Yang, M.; Liu, C. Reconstruction of sparse magnetic anomaly data by integrating spatially adaptive mean compensation with patch based sparse coding. *Meas. Sci. Technol.* **2026**, *37*, 076109. [CrossRef]
21. Schuster, G.T.; Feng, S. Overview of Physics-Informed Machine Learning Inversion of Geophysical Data. *arXiv* **2023**, arXiv:2310.08109.
22. Elshenawy, A.; Mohammed, A.; Hamouda, S. The evolution of deep learning: Models, applications, and future directions. In Proceedings of the 2025 International Mobile, Intelligent, and Ubiquitous Computing Conference (MIUCC), Cairo, Egypt, 17–18 September 2025; pp. 1–8.
23. Annan, R.F.; Wan, X. Recovering bathymetry of the Gulf of Guinea using altimetry derived gravity field products combined via convolutional neural network. *Surv. Geophys.* **2022**, *43*, 1541–1561. [CrossRef]
24. Wan, X.; Annan, R.F.; Ziggah, Y.Y. Altimetry derived gravity gradients using spectral method and their performance in bathymetry inversion using back propagation neural network. *J. Geophys. Res. Solid Earth* **2023**, *128*, e2022JB025785. [CrossRef]

25. Harper, H.; Sandwell, D.T. Global predicted bathymetry using neural networks. *Earth Space Sci.* **2024**, *11*, e2023EA003199. [CrossRef]
26. Zhu, C.; Yang, L.; Bian, H.; Guo, J.; Xiao, C. Recovering gravity from satellite altimetry data using deep learning network. *IEEE Trans. Geosci. Remote Sens.* **2023**, *61*, 1–11. [CrossRef]
27. Li, Q.Q.; Zhai, Z.H.; Bao, L.F.; Wang, Y.; Wu, L.; Mao, G.C.; Sun, H.P. A convolutional neural network to optimize multi mission satellite altimeter fusion for improving the marine gravity field. *Earth Planets Space* **2024**, *76*, 129. [CrossRef]
28. Zhao, H.D.; Zhang, N.; Li, C.S.; Liu, Y. Construction method of geomagnetic reference map for satellite communication navigation through Kriging method. *J. Phys. Conf. Ser.* **2021**, *2033*, 012028. [CrossRef]
29. Zhan, C.; Huang, P.; Xue, B.; Lan, B. A neural network based automatic semi-variogram modeling approach for geomagnetic map construction in multi-source indoor and outdoor navigation. *Sci. Rep.* **2026**, *16*, 1928. [CrossRef] [PubMed]
30. National Marine Data Center. National Science & Technology Resource Sharing Service Platform of China. Available online: https://mds.nmdis.org.cn/ (accessed on 15 November 2025).
31. Auld, D.R.; Law, L.K.; Currie, R.G. Cross over error and reference station location for a marine magnetic survey. *Mar. Geophys. Res.* **1979**, *4*, 167–179. [CrossRef]
32. Saltus, R.W.; Blakely, R.J. Unique Geologic Insights from "Non-Unique" Gravity and Magnetic Interpretation. *GSA Today* **2011**, *21*, 4–10. [CrossRef]
33. Noguchi, Y.; Nakanishi, M.; Ishiharae, T.; Tamaki, K.; Fujimoto, H.; Huchon, P.; Leroy, S.; Styles, P. A Comparison of Two Leveling Methods for Geomagnetic Data. *J. Jpn. Soc. Mar. Surv. Technol.* **2017**, *29*, 3–18.

Disclaimer/Publisher's Note: The statements, opinions and data contained in all publications are solely those of the individual author(s) and contributor(s) and not of MDPI and/or the editor(s). MDPI and/or the editor(s) disclaim responsibility for any injury to people or property resulting from any ideas, methods, instructions or products referred to in the content.